WOOD RESEARCH
63 (2): 2018
179-192

DYNAMIC RELATIONSHIP BETWEEN MECHANICAL PROPERTIES AND CHEMICAL COMPOSITION DISTRIBUTION OF WOOD CELL WALLS

Enhua Xi
Shandong Agricultural University, College of Forestry
Tai'an, China

Institute of Wood Science of Shandong Province
Tai'an, China

(Received March 2018)

ABSTRACT

Wood is a natural composite material with a complex structure. Its mechanical properties are mainly due to the cell walls. In order to investigate the relationship between mechanical properties and chemical composition of wood cell wall. Nanoindentation and Raman imaging were used to characterize the longitudinal mechanical properties and chemical composition distribution of wood fibers of three years old fast-growing poplar (*Populus×euramericana* cv. '74 /76') during the growing season at different times. The results were showed that the content and distribution of cellulose and lignin are closely related to the mechanical properties of wood fiber cell walls, especially the cellulose for the longitudinal elastic modulus and the lignin for the hardness of cell walls. It was also demonstrated that the longitudinal elastic modulus and hardness of the secondary wall 2 layer (S2) were strongly correlated to the micro fibril angle (MFA) and crystallinity of cellulose during the active phase.

KEYWORDS: Mechanical properties, chemical composition, wood cell wall, growing season.

INTRODUCTION

The most important characteristic of wood is its excellent mechanical performance at comparably lower weight in technical application as well as the use of structural material. In order to increase our understanding of the mechanical properties of wood, it is crucial to take into account its distinct structure of the wood cells. On the microscopic level, there are many differences between individual types of cells. Meanwhile, the cell wall of an individual cell is different from the others. A wood cell wall is built-up of layers which differ in their chemical

composition and their structure. Since the S2 layer is the thickest wall layer in wood cell walls, and the most important structural feature of the layer being variable in the MFA and crystallinity, research efforts concentrate on this cell wall region. Nanoindentation, a method of hardness and elastic modulus testing at the micrometer level or even at the nanometer scale, has been increasingly applied in a variety of studies on wood, bamboo and other cellulosic fibers (Gindl et al. 2002, Wu et al. 2010, Yu et al. 2011, Wang et al. 2012). The nanoindentation was first introduced in the field of wood science by Wimmer and Lucas (1997a, 1997b) to estimate the mechanical properties of the secondary wall, the cell corner (CC) and the compound middle lamella (CML) of spruce tracheids. Subsequent investigations were conducted by focused on MFA and lignifications (Gindl et al. 2004) related to longitudinal hardness and elastic modulus of the secondary wall of softwood tracheids. Many applications for nanoindentation in the field of wood research have been demonstrated by recent publications, such as mechanical properties of wood flooring paint films (Jiang et al. 2006), bonding interface of wood-adhesive (Konnerth and Gindl 2006, 2008, Konnerth et al. 2007, Follrich et al. 2010, Stöckel et al. 2010), wood modification, wood fiber polymer composites (Gindl et al. 2006, Lee et al. 2007), creep behavior of lyocell fibers (Lee et al. 2007), and thermo-mechanical refining (Xing et al. 2008).

Some wood scientists have investigated the nano-mechanical properties of wood cell walls by nanoindentation, but the majority of research was focused on their local softwood species such as loblolly pin (Tze et al. 2007, Xing et al. 2009) and spruce (Wimmer et al. 1997, Wimmer and Lucas 1997, Gindl et al. 2004). Only a few references were found for nanomechanical properties of hardwood by nanoindentation (Wu et al. 2009). Hardwood species have more complex wood structure and cellular compositions compared with softwood. About 90-95% of the wood cells in softwood are tracheids, however, in hardwood, apart from wood fiber cell; the number of vessel elements is also high.

Confocal Raman spectroscopy recently has been found in application as chemical mapping and imaging techniques for biological and biomimetic samples (Salzer et al. 2000, Chenery and Bowring 2003). Raman scattering involves excitation of a molecule by inelastic scattering with a photon (from a laser light source) (Schrader 1995) and depends on changes in the polarizability of functional groups due to molecular vibration. Therefore, Raman spectroscopy can provide complementary information about the molecular vibrations. This method has developed as important tool in plant cell wall research (Atalla and Agarwal 1985, Stewart 1996, Himmelsbach et al. 1999, McCann et al. 2001, Morris et al. 2003), as it was allowed to acquire the information about the molecular structure and composition of individual features of plant cells. In combination with microscopy, the advantage of Raman spectroscopy is to obtain a higher spatial resolution on aqueous, thicker samples

In this study, confocal Raman microscopy and nanoindentation were used to characterize the in situ distribution of chemical components and mechanical properties of wood fiber cell walls in fast-growing poplar (Populus×euram ericana cv. '74 /76') during the growing season. The dynamic relationship between mechanical properties and chemical components distribution of the same cell walls were elucidated. The aim of this study was to discover the dynamic microscopic correlation between structure and performance of cell, and further for providing strong biological basis information in controlling and enhancing the macro-mechanical properties of wood.

MATERIAL AND METHODS

Plant material and preparation

Healthy plants of fast-growing 3-year-old *Populus×euramericana* cv. '74/76' grown in a plantation in Beijing's Changping district with the same diameter at breast height were chosen and marked. Plant materials were taken 1.3 m above the ground root level and sampled once a month from May to October. On each occasion, small cubic blocks (about 10 ×10 × 10 mm) containing phloem, cambium, and xylem cells were immediately immersed in fixative formalin–acetic acid–alcohol (FAA) for preserving the material. Upon returning to the laboratory, they were placed in the same fresh fixative under a slight vacuum for 30 min. The pieces were fixed in fresh fixative and preserved at 4°C. The sample block was cut into two halves axially. One half was used for Raman imaging, and the other for nanoindentation testing.

Raman imaging

Without any further sample preparation, 10-μm-thick cross sections including phloem, cambium were cut on a sliding microtome (Leica, RM2000R), and then repeatedly washed with distilled water. Slices were placed on a glass slide with a water drop, and sealed with a cover slip to observe the last formed wood fibers closest to the cambium.

A confocal Raman microscope (XploRA, Horiba Jobin Yvon, France) equipped with a piezo scanner and a microscopic objective from Olympus (100×, NA=1.25) was used to acquired the spectra. A linear polarized green laser (λ=532 nm) was focused with a diffraction-limited spot size (0.61 λ/NA). The Raman light was detected by an air-cooled, back-illuminated spectroscopic CCD (ANDOR) behind a grating (1200 $g \cdot mm^{-1}$) spectrograph (ACTON) with a resolution of 6 cm^{-1}. The scanning data was acquired by a scanning probe with a step of 0.4 μm. The time of a single point acquisition was 6_S, a slit width was 100 μm and a confocal hole size was 300 μm.

In situ imaging nanoindentation testing

The procedure of sample preparation for nanoindentation was similar to that proposed by Wimmer et al. (1997). In brief, the sample sticks were embedded in Spur resin and cured in a plastic mold. After curing, the cross-section of samples was cut with an ultra microtome equipped with a diamond knife to obtain a very smooth surface for indenting. The Triboindenter (Hysitron Incorporation, USA) with a radius less than 100 nm diamond indenter was selected for indenting. The target peak load and loading-unloading rate was 250 μN and 50 $\mu N \cdot s^{-1}$, respectively. The hold time at peak load was 6 s (Yu et al. 2011).

Elastic punch theory states that the elastic modulus of materials and hardness can be inferred from load-displacement curves of nanoindentation. According to the method of Oliver and Pharr (1992), the unloading segment can be fitted very well with a power-law function, from which the initial slope of the unloading curve, namely elastic contact hardness (H), can be determined. Based on H, the reduced elastic modulus E_r can also be obtained. Then the MOE and hardness of materials can be calculated from the following Eq. 1:

$$\frac{1}{E_r} = \frac{1 - v^2}{E} + \frac{1 - v_i^2}{E_i} \quad (1)$$

$$H = \frac{P}{A} \quad (2)$$

where: P - peak load,
A - which can be calculated from an empirical formula, is the projected area at peak load,
E_r - called the reduced elastic modulus,
E_i and v_i - respectively the elastic modulus and Poisson ratio of the tips.

For diamond tips, E_i is 1141 GPa, and vi is 0.07. E and v are, respectively, the elastic modulus and Poisson ratio of samples. It should be pointed out that the modulus E and E_r are almost identical for soft materials like wood, which eliminated the need to obtain the Poisson ratio of the cell wall of wood fibers.

The thickness of wood fiber cell wall is only 2-6 μm. Although the nanoindentation apparatus has high accuracy (indentation depth resolution can reach 0.1 nm), the precision of x-y positioning platform is 1.5 μm/inch. If indenter moves 2.54 cm in a horizontal direction, it will generate the error of 0.1 nm in cell wall. So it cannot fully guarantee each indentation can be very accurate in cell walls, the creasing points need to be determined, to ensure the effectiveness of the indentations, as shown in Fig. 1.

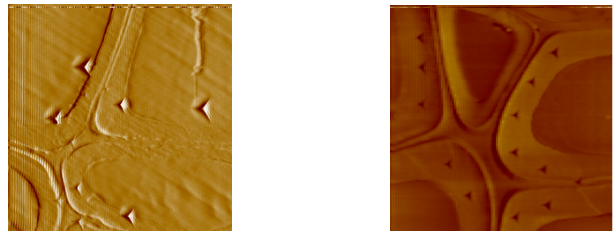

a b

Fig. 1: a. The invalid indentation points. b. The effective indentation points.

The in situ images of nanoindentation points of wood fiber cell wall during the growing season were shown in Fig. 2. Trees were sampled on the 15th of each month.

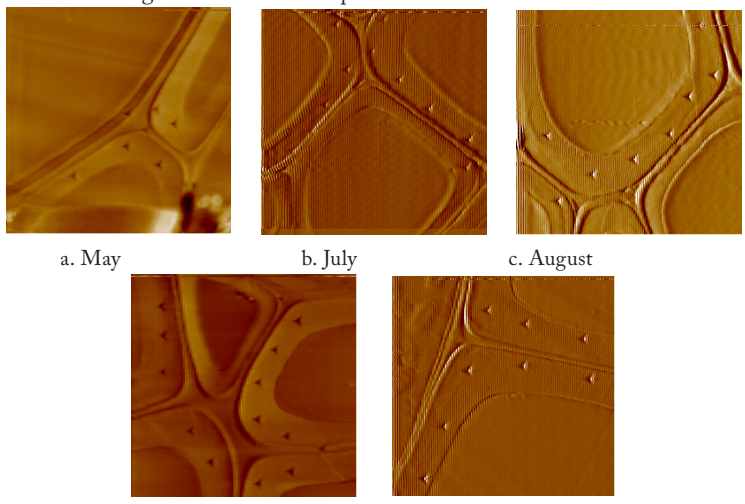

a. May b. July c. August

d. September e. October

Fig. 2: The in situ images of nanoindentation points of wood fiber cell wall in S2 *in different growth phase.*

MFA and crystallinity

A powder X-ray diffractometer (X'Pert Pro, Panalytical, USA) was used to measure the MFA and crystallinity. The specimens were 10(L) ×5(T) mm with a thickness of 0.5(R) mm. The X-ray diffractometer was operated at a voltage of 40 Kv with a current density of 40 mA. The radiation source was a CuKa (λ= 0.154nm). The scanning range was from 2θ=5˚ to 40˚ at a scan speed of $0.084^{\circ}\cdot s^{-1}$ (Yu et al. 2011). The data was collected using a continuous mode with angular intervals of 0.084˚. The obtained scanning intensity curve data was imported into the Origin data processing software, and the MFA was obtained by Gaussian function fitting. The mean MFA was determined according to the method developed by Cave (1966). The same specimens were ground into powder for evaluate the Crystallinity as crystallinity index and determined from the ratio of the intensity of the sample. The formula for crystallinity index, CrI, is as follows:

$$CrI\ (\%) = (I_{002} - I_{am}) / I_{002} \times 100$$

where: I_{002} - the maximum intensity of 002 diffraction peak at 2θ=20.002˚,
I_{am} - the minimum intensity of a peak near 2θ=18.000˚.

RESULTS

Distribution of chemical composition of cell wall layers

The Raman bands used for analysis and their assignment to lignin (L) and cellulose (C) were shown in Tab. 1 (Gierlinger et al. 2006). Two-dimensional chemical images were calculated by integrating over wave number ranges (Figs. 3 and 4) in different active phases (May to October).

Tab. 1: The Raman bands used for analysis and their assignment to lignin (L) and cellulose (C).

Wavenumber (cm^{-1})	Component	Assignment
2.897	C	CH and CH_2 stretching vibration(str.)
1.601	L	Aryl ring str., sym.
1.462	L and C	HCH and HOC bending
1.333	C	HCC and HCO bending
1096	C, Xyl, and GlcMAn	Heavy atom (CC and CO) str.
903	C	Heavy atom (CC and CO) str.

The higher cellulose content can be seen in the peak at about 2.897 cm^{-1} (2.772~3.045 cm^{-1}), dominated by the stretching vibration of CH and CH_2 groups (Tab. 1 and Fig. 5). The spectra were calculated for the different cell wall layers (CC, CML, and S2) of wood fiber cells during the active phase by selecting the distinct areas on the chemical images (Fig. 3 and Fig. 5). It can be clearly observed from Fig. 3 that the distribution of cellulose in the S2 layer was the strongest, indicating that the S2 concentration in the secondary wall is the highest. The weakest cellulose Raman signal was in the CC, indicating the lowest concentration of cellulose in this area. There is a clear difference in Raman signal intensity of cellulose in the CML. It was probably due to the very thin cell walls of the wood fiber, and the Raman spectrometer's lateral resolution was 1 μm. Raman signal of cellulose in CML was covered by the stronger signal in the S2 layer, resulting in a difference in signal intensity. In addition, the molecular orientation of cellulose molecules in different cell layers would also lead to differences in the Raman signal intensity of cellulose. The orientation of the microfibril in the S2 layer of the wood fiber cell is mainly parallel to the axis of

the cell. The 2.897 cm^{-1} peak was caused by the C-H stretching vibration of the methylene group in the cellulose molecule, and the vibration direction of the C-H bond was perpendicular to the direction of the cellulose molecular chain and parallel to the direction of the electric vector of the incident light, which could enhance the Raman signal strength. The difference between the Raman signal intensity of cellulose in the same layer in Fig. 3 might be caused by the irregular surface of the sliced sample in the process of sample preparation.

The S2 layer was observed to have the highest intensity at the peak of 2.897 cm^{-1} and thus higher cellulose concentration than the CC and the CML. The CC was the weakest, indicating that the cellulose concentration is the lowest (Fig. 5). Gierlinger (2006) and Zhang (2012) have obtained the same results, the S2 layer have the highest cellulose concentration, followed by CML and CC.

It can be seen from the spectra that the strong intensity of lignin content was observed around 1.601 cm^{-1} (1.519-1.712), which can be assigned to the aromatic C=C vibration. The spectra were calculated for the different cell wall layers (CC, CML, and S2) of wood fiber cells during the active phase by selecting the distinct areas on the chemical images (Fig. 4 and Fig. 5).

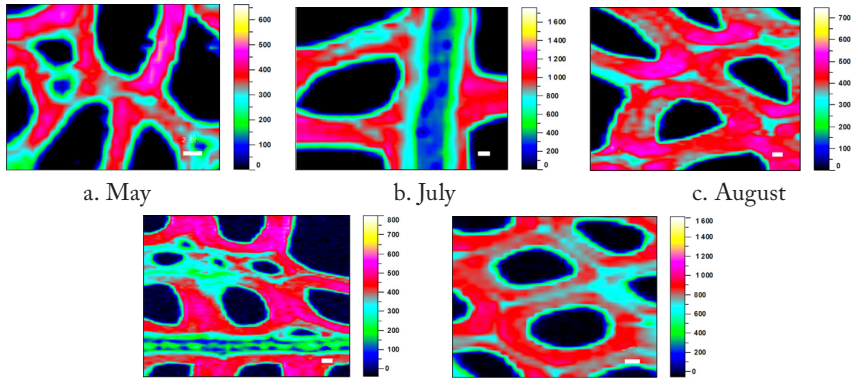

Fig. 3: Raman images of a cross section of wood fiber cells (CC, CML, and S2) showing the cellulose distribution in different stages (2.772– 3.045 cm^{-1}). (Bar = 2um)

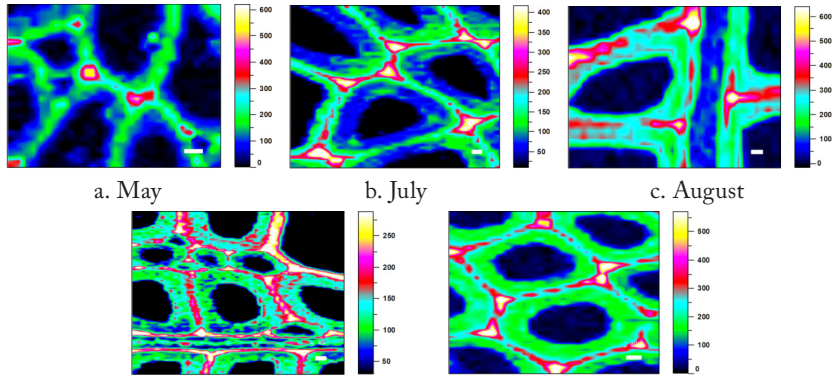

Fig. 4: Raman images of a cross section of wood fiber cells (CC, CML, and S2) showing the lignin distribution in different stages (1.519-1.712 cm^{-1}). (Bar = 2um)

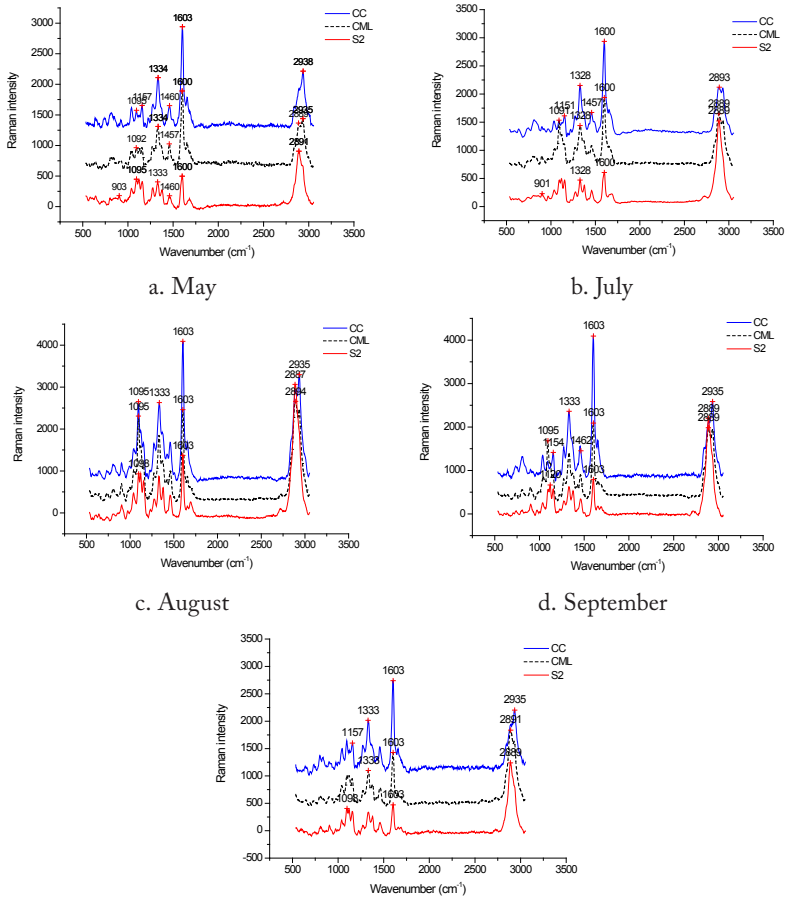

Fig. 5: Raman spectra of S2, CML and CC in different growth stages

In Fig. 4, the CC was discovered to have the strongest Raman signal, indicating that the lignin concentration was the highest. The Raman signal intensity of the CML was slightly lower than that of CC, because of the thin CML and the lateral resolution of the Raman spectrometer. The concentration of lignin in the CML may include multiple cell walls Layers: ML, P, S_1 and S2. The S2 layer was the weakest, demonstrating that the lignin concentration was the lowest. The lignin content was CC > CML > S2, which revealed that the CC had the highest degree of lignification, followed by the CML, the lowest was S2. Gierlinger (2006) found the same results by the research on lignin distribution of *Populus nigra*×*Populus deltoids*. Zhang (2012) showed that the lignin distribution was heterogeneous in the study of the *Daphne odora* Thunb., the highest concentration of lignin in CC, the lower concentration of CML, the lowest concentration in S2, Consistent with the results of this study.

The spectra of S2, CML and CC in different growth stages (May, July, August, September, and October) are shown in Fig. 6. It is observed that the peak at about 2.897 cm^{-1} of the S2,

CML and CC spectrum approximately presented increasing trends from May to October except in August. The highest intensity in the peak at about 2.897 cm^{-1} was in August. The results illustrated that the cellulose content in different parts (S2, CML and CC) of the cell wall was on the whole increased during the active phase. The change in the peak at 1.600 cm^{-1} had the same trend as at 2.795 cm^{-1}. It also demonstrated that the lignin concentration was roughly raised from May to October.

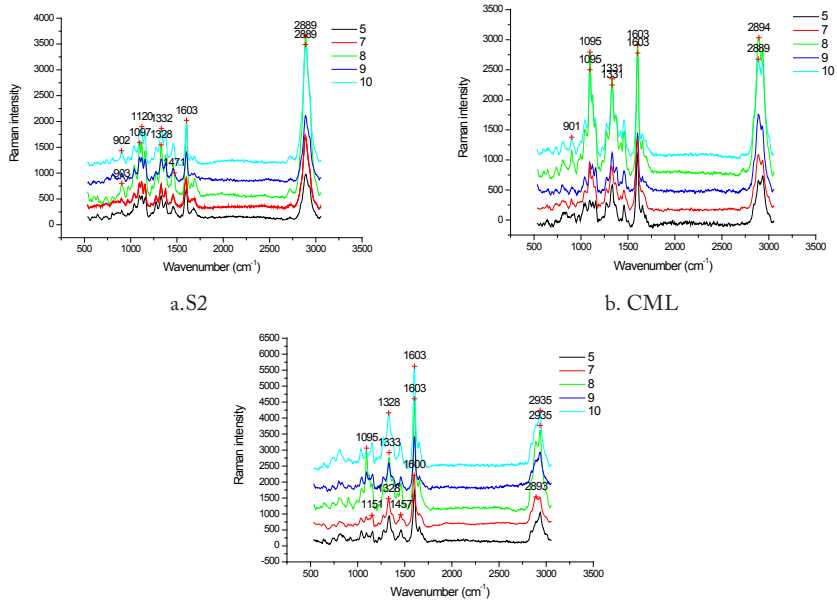

a.S2 b. CML

c. CC

Fig. 6: Raman spectra in different cell wall layers during the active phase.

Mechanical properties of cell wall layers

Fig. 7 shows the elastic modulus of S2, CML, and CC measured with nanoindentation. It can be seen that the longitudinal elastic modulus of wood fiber cell in different position was S2 > CML > CC. The average elastic modulus of S2, CML, and CC were 17-21 GPa, 13-15 GPa, and 9-12 GPa respectively, with an increasing trend during the active phase. The growth rate of elastic modulus from May to October was 23.53%, 15.38%, and 33.33% respectively. If the elastic modulus of CC is defined as a unit, then the ratio of CC, CML and S2 is 1:1.33:1.82. Statistically significant difference was found with changing growing period according to one-way ANOVA (P<0.05).

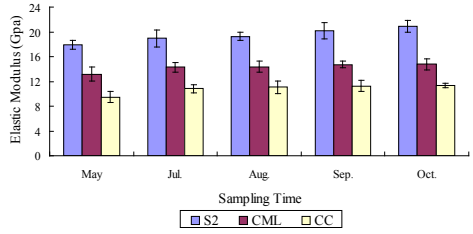

Fig. 7: Histogram of elastic modulus in different cell wall layers during the active phase.

Fig. 8 shows the hardness of S2, CML, and CC measured with nanoindentation. It can be seen that the average longitudinal hardness of S2 was 550-660 MPa, with an increasing trend during the active phase. The growth rate of S2 hardness from May to October was 20.00%. However, the hardness of CC was showed a decreasing tendency from 600 MPa to 520 MPa. The hardness drop rate of CC was 15.38% during the active period. The hardness of CML was not significantly changed and kept at 530-550 Mpa. In the prophase of active phase in May, the longitudinal hardness was CC > CML > S2, however, by the end of active phase in September and October was S2 > CML > CC. No statistically significant difference was found with changing growing period according to one-way ANOVA ($P<0.01$).

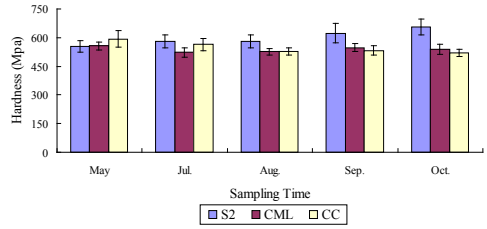

Fig. 8: Histogram of hardness in different cell wall layers during the active phase.

Crystallinity and MFA of cell wall layers

The crystallinity and MFA of the S2 layer during the active phase was measured. It can be seen from the Fig. 9 that the crystallinity of S2 layer was 44.49% to 54.97%, with an increasing trend from May to October. However, the Micro fibril angle of the S2 layer was showed a decreasing tendency from 21.16° to 15.66° (Fig. 10).

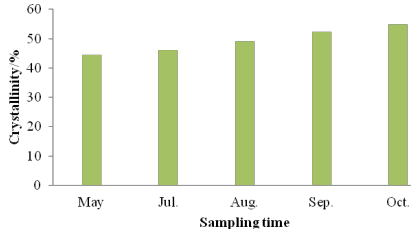

Fig. 9: Crystallinity of S2 layer during the active phase.

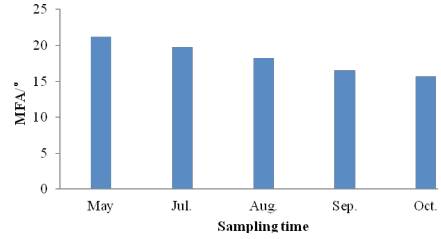

Fig. 10: MFA of the S2 layer during the active phase.

Linear relationship analysis was made between cellulosic characteristics and the mechanical properties of the S2 layer (Tab. 2).

Tab. 2: Correlation coefficients of cellulose with mechanical properties of secondary cell wall.

	E_{S2}	H_{S2}
Cr	0.865*	0.915*
MFA	-0.909*	-0.917*

Note: * Correlation is significant at the 0.05 level (2-tailed)

According to the Pearson's analysis, the results showed that the degree of crystallinity of cellulose had a highly significant positive correlation with the longitudinal elastic modulus and hardness. However, the MFA of cellulose had a highly significant negative correlation with the elastic modulus and hardness of the S2 layer. The same conclusion has been confirmed by many researches (Gindl et al. 2004, Cave 1969, Page et al. 1977, Burgert et al. 2002).

DISCUSSION

Relationship between mechanical properties and cellulose of cell wall

It was found that the cellulose concentration in different parts of wood fiber cell wall was S2> CML> CC in the same period, which had the similar change with the longitudinal elastic modulus of wood fiber. In the meantime, it was found that the cellulose concentration of the S2 layer, the CML and the CC showed a gradually increase tendency during the active period. The change trend of longitudinal elastic modulus of the S2 layer was consistent with that of cellulose concentration. From the results, it can be inferred that the content and distribution of cellulose are closely related to the mechanical properties of cell walls, especially for the longitudinal elastic modulus of cell walls. The higher the cellulose concentration is, the larger the longitudinal elastic modulus of cell walls is.

MFA has been considered an important factor that determines wood properties such as stiffness and strength and it has been shown by Cave (1969) that longitudinal elastic modulus of wood is very much dependent on MFA of S2. On the one hand, conventional wisdom indicates that as the MFA increases (to a value up to 90); the longitudinal stiffness would decrease (Tze et al. 2007). On the other hand, wood bulk density is also strongly related to the mechanical properties of wood (Cown et al. 1999, Evans and Ilic 2001). Contrary to hardness data, changes in cell-wall structure and composition showed a clear effect on the elastic modulus of S2. With increasing MFA and increasing lignin content, the elastic modulus decreased in an s-shaped curve. Model calculations show that, due to low Young's modulus of lignin as compared to the cellulose fibrils, an increasing lignin concentration reduces the elastic modulus of the cell wall, but this effect was found to be minor compared to the strong influence of MFA (Gindl et al. 2004).

Relationship between mechanical properties and lignin of cell wall

The results showed that the lignin concentration in different parts of wood fiber cell wall was CC> CML> S2 in the same period, which was in contrast to the change of the longitudinal elastic modulus, and was consistent with the change of longitudinal hardness in the earlier active stage. The lignin concentration in the S2 layer was increased gradually during the active period, which was kept in line with the change of the longitudinal elastic modulus and the hardness of the S2 layer. The degree of lignification in the CC and CML of earlywood was higher than that of the latewood during the active period, which was consistent with the change of the hardness in CC and CML. From the above results, it can be concluded that the content and distribution of lignin are closely related to the mechanical properties of cell walls, especially for the hardness of cell wall. The higher the lignin concentration is, the higher the longitudinal hardness of cell wall is.

Wimmer (1997) found that the elastic modulus of CML with high lignin content was significantly low compare with that of the secondary cell wall with a lower lignin, they attributed this to the almost completely devoid of cellulose in the zone of CML. On the contrary, the minor differences between hardness of CML and secondary cell wall, which demonstrated that the

hardness was less affected by the lignin content. Gindl (2004) discovered that the lignin content was 0.21 $g \cdot g^{-1}$ of lignified tracheid compared with immature tracheid of 0.10 $g \cdot g^{-1}$, the elastic modulus and hardness were increased by 22% and 26% respectively. Zhang (2011) studied the delignification treatment compared with the untreated cell wall, the elastic modulus lost 6.53% and the hardness decreased 16.98%, which showed that the lignin content and existence for the influence of hardness was larger than that of the elastic modulus.

CONCLUSIONS

Nanoindentation and Raman imaging were used to characterize the longitudinal mechanical properties and chemical composition distribution of wood fibers during the active period. The relationship between mechanical properties and chemical composition was investigated in this study. In short, the following conclusions can be obtained. First, the results of the distribution of chemical constituents in different parts of the same stage during the active period showed that the concentration of lignin was CC> CML> S2, and the relative concentration of cellulose was S2 > CML> CC. The concentration of lignin and cellulose in the S2 layer, CML and CC was increased first and then decreased during the whole active period, and the concentration of latewood cells was higher than that of the early wood ones. Second, the longitudinal elastic modulus in different position was S2 > CML > CC and with an increasing trend. The hardness of the S2 layer showed an increasing trend and CC was a decreasing trend during the active phase. Third, the crystallinity of S2 layer was increased from 44.49% to 54.97%. However, the MFA of the S2 layer was showed a decreasing tendency from 21.16° to 15.66°. The longitudinal elastic modulus and hardness of the S2 layer are mainly dependent on MFA and crystallinity of cellulose. Finally, from the results, it can be concluded that the content and distribution of cellulose and lignin are closely related to the mechanical properties of cell walls, especially cellulose for the longitudinal elastic modulus and lignin for the hardness of cell walls.

ACKNOWLEDGEMENTS

The work was financially supported by the National Natural Science Foundation of China (grant number: 31700485); and the Education department of Shandong province (scientific research project of colleges and universities in Shandong province, grant number: J14LF09).

REFERENCES

1. Atalla, R.H, Agarwal, U.P., 1985: Raman microprobe evidence for lignin orientation in the cell walls of native woody tissue, Science 227(4687): 636-638.
2. Burgert, I., Keckes, J., Fruhmann, K., Fratzl, P., Tschegg, S.E., 2002: A comparison of two techniques for wood fiber isolation evaluation by tensile tests on single fibers with different micro fibril angle, Plant Biology 4(1): 9-12.
3. Cave, I.D., 1966: Theory of X-ray measurement of microfibril angle in wood, Forest Products Journal 16: 37-42.
4. Cave, I.D., 1969: The longitudinal Young's modulus of *Pinus radiata*, Wood Science and Technology 3(1): 40-48.

5. Chenery, D., Bowring, H., 2003: Infrared and Raman spectroscopic imaging in bioscience, Spectroscopy Europe 15: 8-14.
6. Cown, D.J., Herbert, J., Ball, R.D., 1999: Modeling *Pinus radiata* lumber characteristics. Part 1: Mechanical properties of small clears. New Zealand Journal of Science 29(2): 203-213.
7. Evans, R., Ilic, J., 2001: Rapid prediction of wood stiffness from micro fibril angle and density, Forest Products Journal 51: 53-57.
8. Follrich, J., Stöckel, F., Konnerth, J., 2010: Macro- and micromechanical characterization of wood-adhesive bonds exposed to alternating climate conditions, Holzforschung 64: 705-711.
9. Gierlinger, N., Schwanninger, M., 2006: Chemical imaging of poplar wood cell walls by confocal raman microscopy, Plant Physiology 140(4): 1246-1254.
10. Gindl, W., Gupta, H.S., Grünwald, C., 2002: Lignification of spruce tracheid secondary cell walls related to longitudinal hardness and modulus of elasticity using nano-indentation, Canadian Journal of Botany 80(10): 1029-1033.
11. Gindl, W., Gupta, H.S., Stöckel, T., Lichtenegger, H.C., Fratzl, P., 2004: Mechanical properties of spruce wood cell walls by nanoindentation, Applied Physics A 79(8): 2069-2073.
12. Gindl, W., Schoberl, T., Keckes, J., 2006: Structure and properties of pulp fiber-reinforced composite with regenerated cellulose matrix, Applied Physics A 83(1): 19-22.
13. Himmelsbach, D.S., Khahili, S., Akin, D.E., 1999: Near-infrared-Fourier-transform-Raman microspectroscopic imaging of flax stems, Vibrational Spectroscopy 19(2): 361-367.
14. Jiang, Z.H., Yu, Y., Qin, D.C., Wang, G., Zhang, B., Fu, Y.J., 2006: Pilot investigation of the mechanical properties of wood flooring paint films by in situ imaging nanoindentation, Holzforschung 60: 698-701.
15. Konnerth, J., Gindl, W., 2006: Mechanical characterization of wood-adhesive interphase cell walls by nanoindentation, Holzforschung 60: 429-433.
16. Konnerth, J., Valla, A., Gindl, W., 2007: Nanoindentation mapping of a wood-adhesive bond, Applied Physics A 88: 371-375.
17. Konnerth, J., Gindl, W., 2008: Observation of the influence of temperature on the mechanical properties of wood adhesives by nanoindentation, Holzforschung 62:714-717.
18. Lee, S.H., Wang, S.Q., Pharr, G.M., Xu, H.T., 2007: Evaluation of interphase properties in a cellulose fiber-reinforced polypropylene composite by nanoindentation and finite element analysis, Composites Part A: Applied Science and Manufacturing 38(6): 1517-1524.
19. Lee, S.H., Wang, S.Q., Pharr, G.M., Kant, M., Penumadu, D., 2007: Mechanical properties and creep behavior of lyocell fibers by nanoindentation and nano-tensile testing. Holzforschung 61: 254-260.
20. McCann, M.C., Bush, M., Milionia, D.,Sadoa, P., Stacey, N.J., Catchpole, G., Defernez, M., Carpita, N.C., Hoft, H., Ulvskov, P., et al., 2001: Approaches to understanding the functional architecture of the plant cell wall, Phytochemistry 7(6): 811-821.
21. Morris, V.J., Ring, S.G., MacDougall, A.J., Wilson, R.H., 2003: Biophysical characterisation of plant cell walls. In: The Plant Cell Wall-Annual Plant Reviews (ed. Rose J)., Oxford, Pp 55-91.
22. Oliver, W.C., Pharr, G.M., 1992: An improved technique for determining hardness and elastic modulus using load and displacement sensing indentation experiments, Journal of Materials Research 7(6): 1564-1583.

23. Page, D.H., El-Hosseiny, F., Winkler, K., Lancaster, A.P., 1977: Elastic modulus of single wood pulp fibers, TAPPI 60(4):114-117.
24. Salzer, R., Steiner, G., Mantsch, H.H., Mansfield, J., Lewis, E.N., 2000: Infrared and Raman imaging of biological and biomimetic samples, Fresenius Journal of Analytical Chemistry 366(6-7): 712-726.
25. Schrader, B., 1995: Infrared and Raman Spectroscopy: Methods and applications, ed. B.H VCH, Weinham, Germany.
26. Stewart, D., 1996: Fourier transform infrared microspectroscopy of plant tissues. Applied Spectroscopy 50(3): 357-365.
27. Stöckel, F., Konnerth, J., Kantner, W., Moser, J., Gindl, W., 2010: Tensile shear strength of UF- and MUF-bonded veneer related to data of adhesives and cell walls measured by nanoindentation, Holzforschung 64: 337-34.
28. Tze, W.T.Y., Wang, S., Rials, T.G., Pharr, G.M., Kelley, S.S., 2007: Nanoindentation of wood cell walls: continuous stiffness and hardness measurements. Composites Part A, Applied Science and Manufacturing 38(3): 945-953.
29. Wang, X.Q., Ren, H.Q., Zhang, B., Fei, B.H., Burgert, I., 2012: Cell wall structure and formation of maturing fibers of moso bamboo (*Phyllostachys pubescens*) increase buckling resistance, Journal of the Royal Society Interface 9(70): 988-996.
30. Wimmer, R., Lucas, B.N., 1997: Comparing mechanical properties of secondary wall and cell corner middle lamella in spruce wood, IAWA Journal 18(1): 77-88.
31. Wimmer, R., Lucas, B.N., Tsui, T.Y., Oliver, W.C., 1997: Longitudinal hardness and Young's modulus of spruce tracheid secondary walls using nanoindentation technique, Wood Science and Technology 31(2): 131-141.
32. Wu, Y., Wang, S., Zhou, D., Xing, C., Zhang, Y., 2009: Use of nanoindentation and silviscan to determine the mechanical properties of 10 hardwood species, Wood and fiber science 41(2): 64-73.
33. Wu, Y., Wang, S., Zhou, D., Xing, C., Zhang, Y., Cai, Z., 2010: Evaluation of elastic modulus and hardness of crop stalks cell walls by nano-indentation, Bioresource Technology 101: 2867-2871.
34. Xing, C., Wang, S., Pharr, G.M., Groom, L.H., 2008: Effect of thermo-mechanical refining pressure on the properties of wood fibers as measured by nanoindentation and atomic force microscopy, Holzforschung 62: 230-236.
35. Xing, C., Wang, S., Pharr, G.M., 2009: Nanoindentation of juvenile and mature loblolly pine (*Pinus taeda* L.) wood fibers as affected by thermomechanical refining pressure, Wood Science and Technology 43: 615-625.
36. Yu, Y., Tian, G.L., Wang, H., Fei, B.H., Wang, G., 2011: Mechanical characterization of single bamboo fibers with nanoindentation and microtensile technique, Holzforschung 65: 113-119.
37. Zhang, S.Y., 2011: Research on the chemical components affect on mechanics performance of wood cell wall. PhD thesis, Beijing.
38. Zhang, Z. H., 2012: Confocal Ranman microspectroscopy study on the distribution of cellulose and lignin in Daphne odora Thunb, Spectroscopy and Spectral Analysis 32(4): 1002-1006.

Enhua Xi*
Shandong Agricultural University
College of Forestry
Tai'an 271018
China

Institute of Wood Science of Shandong Province
Tai'an 271018
China
*Corresponding authors: xienhua@126.com